Interface strength and crack propagation mechanisms in sintered copper nanoparticles

Du, Leiming; Jiao, Weiping; Bäcke, Olof; Colliander, Magnus Hörnqvist; Poelma, René H.; Fan, Jiajie; van Driel, Willem D.; Fan, Xuejun; Zhang, Guoqi

DOI
10.1016/j.actamat.2025.121187

Licence
CC BY

Publication date
2025

Document Version
Final published version

Published in
Acta Materialia

Citation (APA)
Du, L., Jiao, W., Bäcke, O., Colliander, M. H., Poelma, R. H., Fan, J., van Driel, W. D., Fan, X., & Zhang, G. (2025). Interface strength and crack propagation mechanisms in sintered copper nanoparticles. *Acta Materialia*, *296*, Article 121187. https://doi.org/10.1016/j.actamat.2025.121187

Acta Materialia 296 (2025) 121187

Contents lists available at ScienceDirect

Acta Materialia

journal homepage: www.elsevier.com/locate/actamat

Full length article

Interface strength and crack propagation mechanisms in sintered copper nanoparticles

Leiming Du [a], Weiping Jiao [a], Olof Bäcke [b], Magnus Hörnqvist Colliander [b], René H. Poelma [a,*], Jiajie Fan [c,*], Willem D. van Driel [a], Xuejun Fan [d], Guoqi Zhang [a]

[a] Department of Microelectronics, Delft University of Technology, Mekelweg 4, Delft, 2628 CD, The Netherlands
[b] Department of Physics, Chalmers University of Technology, Kemigården 1, Gothenburg, 412 96, Sweden
[c] Shanghai Engineering Technology Research Center for SiC Power Device, Academy for Engineering & Technology, Fudan University, 220 Handan Rd., Shanghai, 200433, China
[d] Department of Mechanical Engineering, Lamar University, P.O. Box 10028, Beaumont, TX 77710, USA

ARTICLE INFO

Keywords:
Sintering Cu nanoparticles
Interface strength
Micro-cantilever bending test
Transmission Kikuchi diffraction
Cohesive zone model

ABSTRACT

This study investigates the interface strength and fracture behavior of sintered copper (Cu) nanoparticles (NPs) for all-Cu integration in advanced microelectronics packaging. Micro-cantilever bending tests on three configurations (Cu NP-notched, interface-notched and un-notched micro-cantilevers) were analyzed using scanning electron microscopy (SEM), transmission electron microscopy (TEM), transmission Kikuchi diffraction (TKD) and cohesive zone model (CZM). The interface-notched micro-cantilevers demonstrate superior fracture resistance, with a stress intensity factor (K_Q) of 2.88 ± 0.10 MPa $m^{1/2}$, compared to 2.12 ± 0.11 MPa $m^{1/2}$ for Cu NP-notched micro-cantilevers. Simulation results, consistent with experimental results, reveal that Cu NP-notched micro-cantilevers exhibit lower fracture resistance due to porosity and stress concentrations, while interface-notched micro-cantilevers show enhanced strength, attributed to robust bonding and reduced void distribution. Un-notched micro-cantilevers display superior load-bearing capacity, with cracks bypassing the interface and propagating through porous regions. Moreover, in un-notched micro-cantilevers, a synergistic deformation mechanism is observed, where crack propagation through the sintered Cu NPs coexists with plastic slip deformation in the Cu substrate. These findings highlight the strong interfacial bonding and effective stress transfer at the Cu substrate-sintered Cu NP interface, validating the feasibility of direct sintering using Cu NPs without additional coatings.

1. Introduction

All-copper (Cu) integration utilizing Cu nanoparticles (NPs) has emerged as a promising technology for both advanced 3D integration [1–4] and power electronics packaging [5–7]. In 3D integration, direct Cu-to-Cu bonding with sub-10 μm offers superior interconnect density and enhanced electromigration resistance compared to conventional solder-based interconnects [8–10]. However, traditional bulk Cu bonding necessitates high temperatures (>300 °C) and substantial pressures, which pose risks of dielectric layer degradation, particularly in large-scale applications. In contrast, Cu NPs-based bonding enables scalable integration at significantly reduced thermal budgets (160–250 °C) and pressures through nanoscale sintering. Recent studies [2,4] indicate that Cu NPs achieve robust mechanical strength (60 MPa) without requiring costly chemical mechanical polishing (CMP), outperforming conventional thermo-compression bonding in process scalability and surpassing solder-based joints in thermal stability. Furthermore, direct sintering using Cu NPs onto a Cu substrate obviate the requirement for silver (Ag) or nickel (Ni) coating layers in power electronics packaging, offering comparable adhesion performance while reducing material costs [11,12]. Despite these advantages, the large-scale industrial implementation of all-Cu integration using Cu NPs remains limited due to insufficient quantitative data on their interfacial reliability, particularly at the microscale level. This study addresses this critical gap by employing micro-cantilever bending tests to quantitatively assess interface strength, elucidating fracture behaviors that are essential for real-world packaging applications.

Micro-cantilever bending tests have become a widely used technique for evaluating interface strength and fracture toughness at the microscale, providing critical insights into localized deformation and failure mechanisms [13–22]. These tests are particularly effective for

* Corresponding authors.
E-mail addresses: rene.poelma@nexperia.com (R.H. Poelma), jiajie_fan@fudan.edu.cn (J. Fan).

https://doi.org/10.1016/j.actamat.2025.121187
Received 19 January 2025; Received in revised form 28 April 2025; Accepted 28 May 2025
Available online 13 June 2025

probing material interfaces due to their ability to simulate stress states involving both tensile and compressive loading, making them ideal for quantifying interfacial adhesion and mechanical reliability. For example, Matoy et al. [13] applied micro-cantilever bending tests to investigate the fracture behavior of thin-film interfaces, successfully determining energy release rates and critical stress intensities for SiO_2-metal interfaces. Heuer et al. [21] extended this approach to functionally graded materials, demonstrating its applicability for characterizing fracture toughness in heterogeneous systems. Additionally, Armstrong et al. [23] employed micro-cantilever tests to evaluate embrittled grain boundaries in Cu, showcasing its utility in detecting localized failure mechanisms.

Despite these advancements, studies on sintered Cu NPs remain limited. Extensive research has focused on in-situ tensile [24,25], micropillar [26] and compression tests [27,28] to investigate the mechanical properties and deformation mechanisms of sintered silver (Ag) and Cu NPs. These studies have provided valuable insights into viscoplasticity, creep behavior and microstructural evolution under loading. However, they have largely overlooked the interface strength of Cu NPs, particularly under bending conditions, leaving a critical gap in the understanding of interfacial fracture mechanisms. Liu et al. [29] examined Cu-Cu joints fabricated via low-temperature sintering of Cu NPs and highlighted the role of metallurgical bonding and sintered neck formation in enhancing mechanical strength. While their work primarily focused on bulk shear strength, quantitative characterization of localized interfacial fracture properties remains unexplored. This gap in the literature motivates the present study, which aims to provide a detailed understanding of the mechanical reliability and fracture behavior of sintered Cu NPs and their interfaces using micro-cantilever bending tests. These insights are critical for advancing all-Cu integration technologies in microelectronics and structural applications.

Crack propagation in sintered NPs is critically influenced by pore distribution, grain boundaries, and microstructural heterogeneities. Consequently, computational modeling of fracture in such systems necessitates methods capable of resolving complex crack paths while accounting for material stochasticity. To address this challenge, several approaches have been developed, including phase-field fracture model [30–37], extended finite element method (XFEM) [38–42], discrete element method (DEM) [43–46], and the cohesive zone model (CZM) [47–50]. Phase-field fracture model, which represent cracks as diffuse interfaces via energy minimization principles, excel in simulating arbitrary crack nucleation, branching, and coalescence in heterogeneous media—a key feature for sintered NPs with stochastic porosity [51]. However, phase-field model lacks explicit interface elements, limiting their ability to simulate interfacial failure propagation [52,53]. XFEM supports discrete crack growth without remeshing and incorporates plasticity, making it suitable for ductile fracture analysis [38]. Nonetheless, its reliance on predefined enrichment functions limits its applicability in systems with unpredictable crack paths [54], and it faces difficulties in modeling crack branching and merging due to the need for explicit geometric representation of discontinuities [55]. DEM, ideal for granular fragmentation and flow simulations, struggles with continuum-scale stress field resolution and thermo-elasto-plastic coupling, compounded by prohibitive computational costs for large-scale microstructures [56]. In contrast, CZM are particularly well-suited for simulating interfacial crack propagation in sintered Cu NPs, as they explicitly model decohesion at material interfaces through traction–separation laws [48,49]. This approach enables precise modeling of interface failure mechanisms, addressing critical gaps in phase-field and XFEM frameworks for heterogeneous systems with complex interfacial interactions.

This study investigates the interface strength and fracture behavior of sintered Cu NPs to assess their potential for all-Cu integration in advanced microelectronic applications. Micro-cantilever bending tests are conducted to evaluate localized deformation and fracture toughness at the interface, highlighting its critical role in ensuring mechanical reliability. Detailed microstructure characterization using scanning electron microscopy (SEM), transmission electron microscopy (TEM) and transmission Kikuchi diffraction (TKD) reveals the influence of sintered neck formation and porosity on stress transfer and crack resistance. Furthermore, CZM is employed to simulate crack propagation and stress distributions, providing insights into damage evolution and interface defects. These findings offer a deeper understanding of the mechanical behavior and reliability of sintered Cu interfaces, supporting the development of all-Cu integration for next-generation microelectronics.

2. Experimental and simulation method

2.1. Micro-cantilever fabrication

A die-attach structure, consisting of an aluminum (Al) film, a sintered Cu nanoparticle (NP) layer and a Cu substrate was fabricated using pressure-assisted sintering technology [57]. First, the Cu NP paste was uniformly printed onto a Cu substrate using an automatic screen-printing system and a steel stencil with a thickness of 100 μm (Fig. 1a). Then, the printed paste was dried in a nitrogen atmosphere at 120 °C for 5 min to remove organic solvents. Subsequently, an Al film was applied to the surface of the dried Cu paste to substitute the Cu dummy die, facilitating its removal after the sintering process. Pressure-assisted sintering (Fig. 1b) was performed at 250 °C under 20 MPa uniaxial stress for 5 min in a reducing atmosphere (5% H_2/N_2). After sintering, the samples were cooled to room temperature before removing the Al film and sectioning the samples along the centerline using a diamond saw (Fig. 1c). The sintered samples were then prepared for micro-cantilever fabrication.

Micro-cantilever bending tests provide an effective approach for probing the microscale mechanical properties of sintered Cu NPs. Figs. 1d-f illustrates the design and fabrication of three types of micro-cantilevers (Cu NP-notched, interface-notched and un-notched) used in this study. These micro-cantilevers were designed to investigate fracture behavior under different conditions, with each configuration targeting specific material interfaces and regions of interest. In Fig. 1d, the first micro-cantilever is fabricated entirely within the sintered Cu NP region and includes a notch at the base of the cantilever to assess crack initiation and propagation. The geometric parameters, including length (L), width (W), height (B), and length of notch/interface to nanoindenter (L_b), along with the notch length (a), were carefully controlled during fabrication to ensure consistency. Fig. 1e shows the second configuration, where the micro-cantilever spans the interface between the sintered Cu NPs and the Cu substrate. A notch was introduced at the interface to investigate the interfacial strength and crack propagation behavior. Fig. 1f illustrates the third configuration, which also spans the Cu NP–substrate interface but without a notch, enabling the evaluation of intrinsic material deformation and failure mechanisms without pre-existing flaws. The micro-cantilevers were fabricated using a focused ion beam (FIB) milling process. The fabrication steps involved milling U-shaped trenches, tilting and rotating for undercutting, polishing for symmetry, and final cleaning to reduce damage [58]. The dimensions of all micro-cantilevers were determined through SEM images and are presented in Table S1. Notably, a consistent dimensional variation of approximately ±0.2 μm was observed across the micro-cantilevers, demonstrating good reproducibility in their fabrication.

2.2. Micro-cantilever bending tests

Micro-cantilever bending tests were conducted at room temperature using an in-situ nanoindenter system (Alemnis AG, Switzerland) integrated into a Zeiss Ultra55 FEG-SEM (Fig. 2a) [59]. Representative SEM images of the three micro-cantilevers are presented in

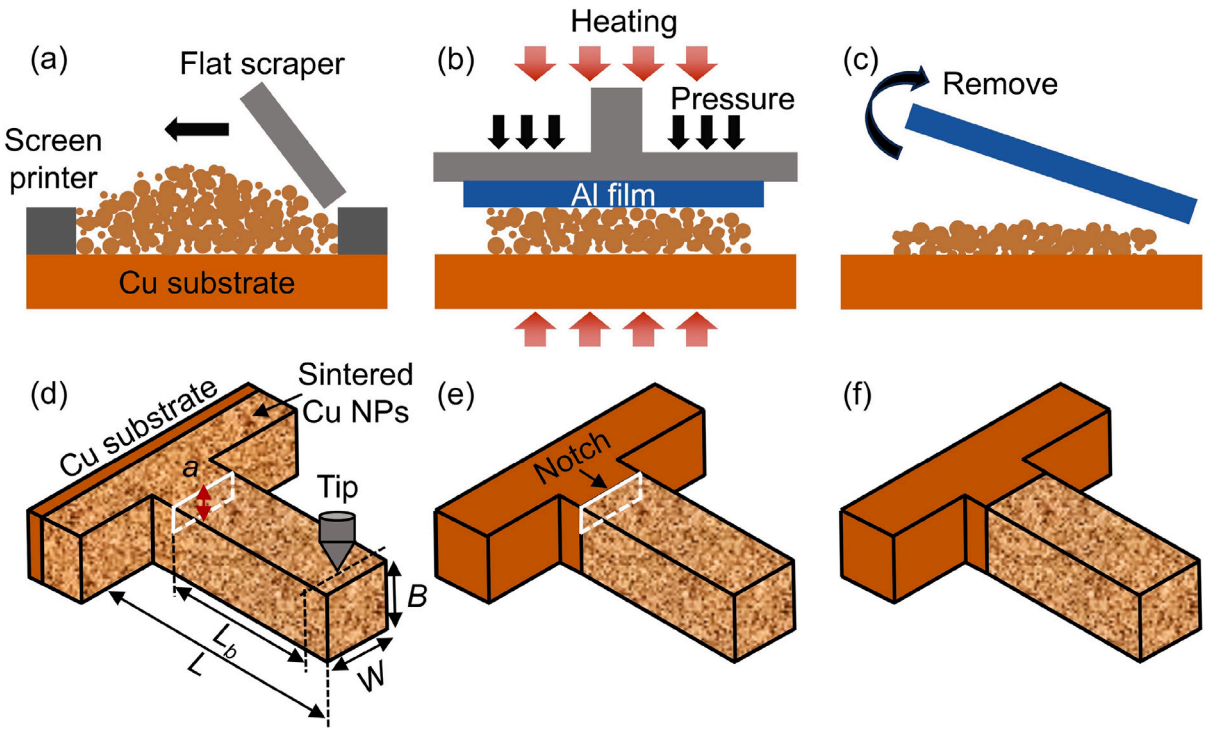

Fig. 1. Sintering process: (a) screen printing; (b) pressure-assisted sintering; (c) removal of the Al film. Schematic of micro-cantilevers: (d) Cu NP-notched micro-cantilever; (e) interface-notched micro-cantilever; (f) un-notched micro-cantilever.

Figs. 2b–d, while the complete set of images for all micro-cantilevers is provided in Fig. S1. Prior to testing, the SEM was employed to precisely align the indenter tip with the fiducial mark located on the top surface of each micro-cantilever. The bending tests were conducted in displacement-controlled mode, maintaining a constant displacement rate of 10 nm s^{-1} for all specimens. The tests proceeded until fracture was observed, ensuring consistent testing conditions. A conospherical diamond tip (radius = 1 μm) was utilized to apply the bending load, as shown. Compared to sharp-tipped indenters, such as the Berkovich indenter, the conical geometry with a spherical tip was selected to minimize stress concentrations and reduce indentation-induced surface damage, thereby improving the accuracy of mechanical property measurements [16]. The nanoindenter system provided high-resolution displacement tracking with drift rates maintained below 10 nm/min, enabling reliable acquisition of load–displacement data. Throughout the experiments, synchronized video recordings and SEM image sequences were captured to continuously monitor the deformation process, facilitating correlation between the applied displacement, measured load and the progression of crack initiation and propagation. This experimental setup ensured precise measurements of mechanical behavior while minimizing artifacts associated with tip geometry and system drift.

2.3. 3D reconstruction

To investigate the internal microstructure of sintered Cu NPs, FIB-SEM tomography was performed using a dual-beam FEI Helios G4 CX system [60]. Prior to milling, a protective Pt layer (1 μm thick) was deposited over the region of interest (ROI), and fiducial markers were fabricated to ensure precise alignment during sequential milling (Fig. 3a). The sample was tilted to 52° to enable perpendicular FIB milling at 30 kV and 40 pA, while SEM imaging was conducted at 10 kV using a secondary electron detector. A U-shaped trench was milled adjacent to the ROI to accommodate redeposited material. Automated slicing and imaging were controlled via Auto Slice and View software, generating 15 nm-thick cross-sectional slices. Approximately 300 high-resolution SEM images were acquired (Fig. 3b), and processed using Avizo software for 3D reconstruction [61]. Image alignment and threshold-based segmentation revealed porous regions (highlighted in blue, Fig. 3c), with a calculated porosity of approximately 10.5%. The reconstructed volume of 6 × 3.5 × 4 μm^3 (Fig. 3d) effectively captured the sintered Cu NP domain and void distribution, demonstrating sufficient representativeness to resolve microstructural features.

2.4. TEM and TKD characterization

The localized deformation behavior and grain orientation of sintered Cu NPs were characterized using TEM (Cs-corrected Titan Themis) and TKD (Zeiss GeminiSEM 360 and Hitachi Regulus8230). TKD was prioritized over conventional electron backscatter diffraction (EBSD) due to its enhanced spatial resolution ($\lesssim$ 5nm), sensitivity to weak crystallographic signals, and compatibility with ultrathin specimens—critical advantages for resolving nanocrystalline microstructures [62, 63]. This technique enabled precise mapping of grain orientations and strain distributions in both as-sintered and deformed interfacial regions, providing insights into plasticity mechanisms at the nanoscale.

2.5. Random porous structure modeling

The porous structures of sintered Cu NPs exhibit inherent randomness in pore size, shape and distribution due to particle rearrangement and coalescence during the sintering process. From a microstructural perspective, sintered Cu NPs can be conceptually represented as a two-phase solid system comprising metallic particles and distributed pores [64]. Accurate modeling of random porous structures is essential for capturing the stochastic characteristics of sintered Cu NPs. To accurately capture this stochastic nature, a Gaussian Random Field (GRF)-based approach was employed to simulate the two-dimensional microstructures [36,37,65–67]. The GRF method effectively models spatial heterogeneity by defining a random field $Z(x)$ through a mean function $m(x)$ and a covariance function $C(x_1, x_2)$. In this study, the

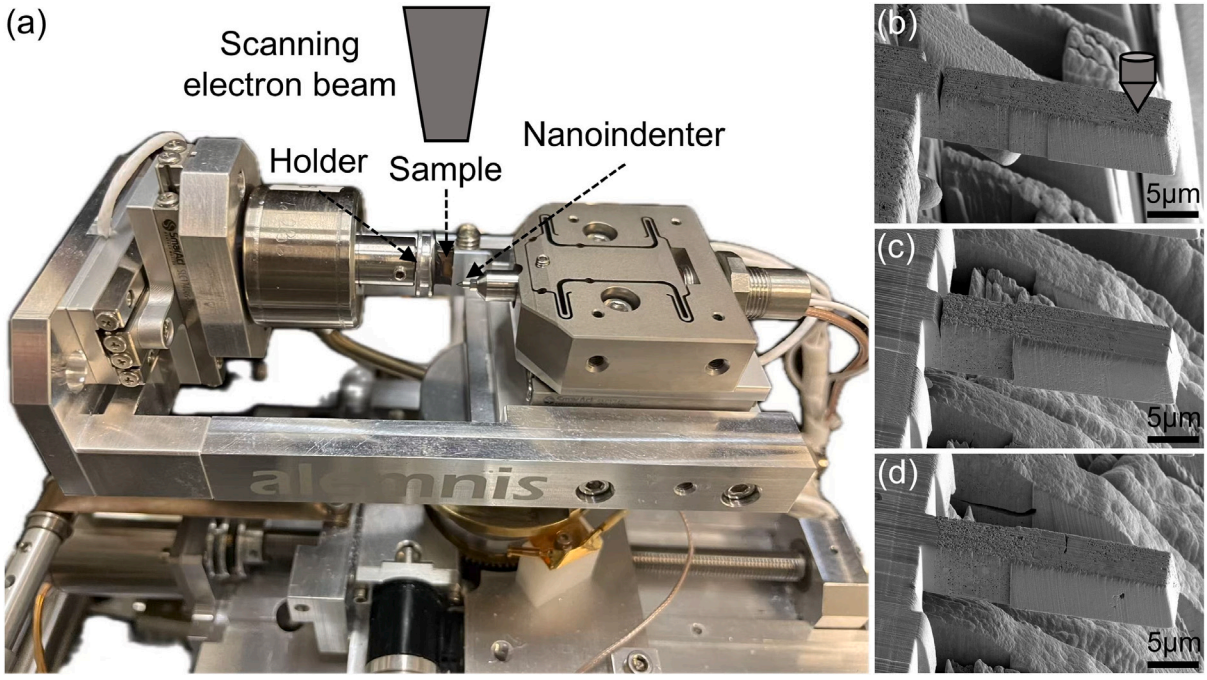

Fig. 2. (a) In-situ SEM setup with indenter; (b–d) representative SEM images of Cu NP-notched micro-cantilever, interface-notched micro-cantilever, and un-notched micro-cantilever, respectively.

mean function was set to zero ($m(x) = 0$) to ensure spatial neutrality, while an exponential covariance function controlled the spatial correlation of the random field. The covariance function is expressed as:

$$C(x_1, x_2) = \sigma^2 \exp\left(-\frac{\|x_1 - x_2\|}{l}\right), \tag{1}$$

where σ^2 represents the variance and l determines the correlation length. A threshold function F_0 was applied to classify the GRF values into solid and pore phases, enabling direct control over porosity. The indicator function $\Psi(x)$ used to separate the phases is given by:

$$\Psi(x) = \begin{cases} 1, & Z(x) \geq F_0, \\ 0, & Z(x) < F_0, \end{cases} \tag{2}$$

This probabilistic framework allowed the generation of pore distributions that closely resemble the experimental microstructures observed in SEM and TEM analyses of sintered Cu NPs. The computational implementation of the GRF model was performed on a 2D square domain of size 160×760 with fine grid discretization to ensure spatial accuracy. Initially, random values following a Gaussian distribution were assigned to each grid point. Gaussian smoothing was then applied to introduce spatial correlations, with the kernel width and correlation length calibrated to control pore size distributions. The smoothed field was converted into binary solid and pore regions using a threshold function, and the resulting structures were meshed to facilitate mechanical simulations (Figs. 4b-d). This process enabled precise adjustments to porosity and morphology, matching experimental observations.

2.6. Cohesive zone model

In this study, the crack propagation behavior of sintered Cu NPs was simulated using a classical bilinear traction–separation law within the Cohesive Zone Model (CZM) framework [48,68], as illustrated in Fig. 4a. The constitutive relation is characterized by two critical displacement parameters: the critical separation displacement (δ_c), corresponding to the peak traction ($\tau_{\max}$), and the ultimate failure separation displacement (δ_t). The critical fracture energy, equivalent to the area under the traction–separation curve, serves as a fundamental parameter governing material failure. For the pure mode I fracture conditions examined here, the cohesive zone response is defined exclusively by $\tau_{\max}$ and δ_t. This simplification arises from the assumption of a constant tangent stiffness (k_1) during the elastic loading phase prior to damage initiation, ensuring a bilinear constitutive response without additional variables influencing the pre-failure regime. k_1 and k_2 are the interface stiffness which are computed as $k_1 = \tau_{\max}/\delta_c$ and $k_2 = \tau_{\max}/(\delta_t - \delta_c)$.

$$\tau(\delta) = \begin{cases} k_1\delta & 0 \leq \delta \leq \delta_c \\ k_2(\delta - \delta_t) & \delta_c \leq \delta < \delta_t \\ 0 & \delta \geq \delta_t \end{cases} \tag{3}$$

As shown in Figs. 4b-d, 2D models with randomly distributed pores is used to simulate the mechanical properties and fracture behavior. The dimension of the model is 4.8 μm × 22.5 μm with quadrilateral elements of 0.03 μm × 0.03 μm. The green regions correspond to the Cu material, while the white regions represent voids, simulating the porosity inherent in the material after sintering. Fig. 4b-d shows the three finite element mesh (4 nodes CPS4) structures, namely, Cu NP-notched, interface-notched and un-notched micro-cantilevers. The initial crack length of the notched micro-cantilevers was set as 2 μm. Bend loading was applied along the right edge (denoted by directional arrows) to simulate bending stress conditions. The mechanical properties for our simulations were directly extracted from the experimental stress–strain curves presented in Fig. 5b.

3. Results and discussion

3.1. Mechanical properties

Fig. 5a presents the load–displacement curves for the micro-cantile vers. The experimentally recorded loading and displacement data of un-notched micro-cantilevers can be transformed into bending stress and bending strain, respectively, through the following equations [69–71]:

$$\sigma = \frac{4 \cdot F \cdot L_b}{W \cdot B^2} \tag{4}$$

$$\varepsilon = \frac{3 \cdot B \cdot u}{2 \cdot L_b^2} \tag{5}$$

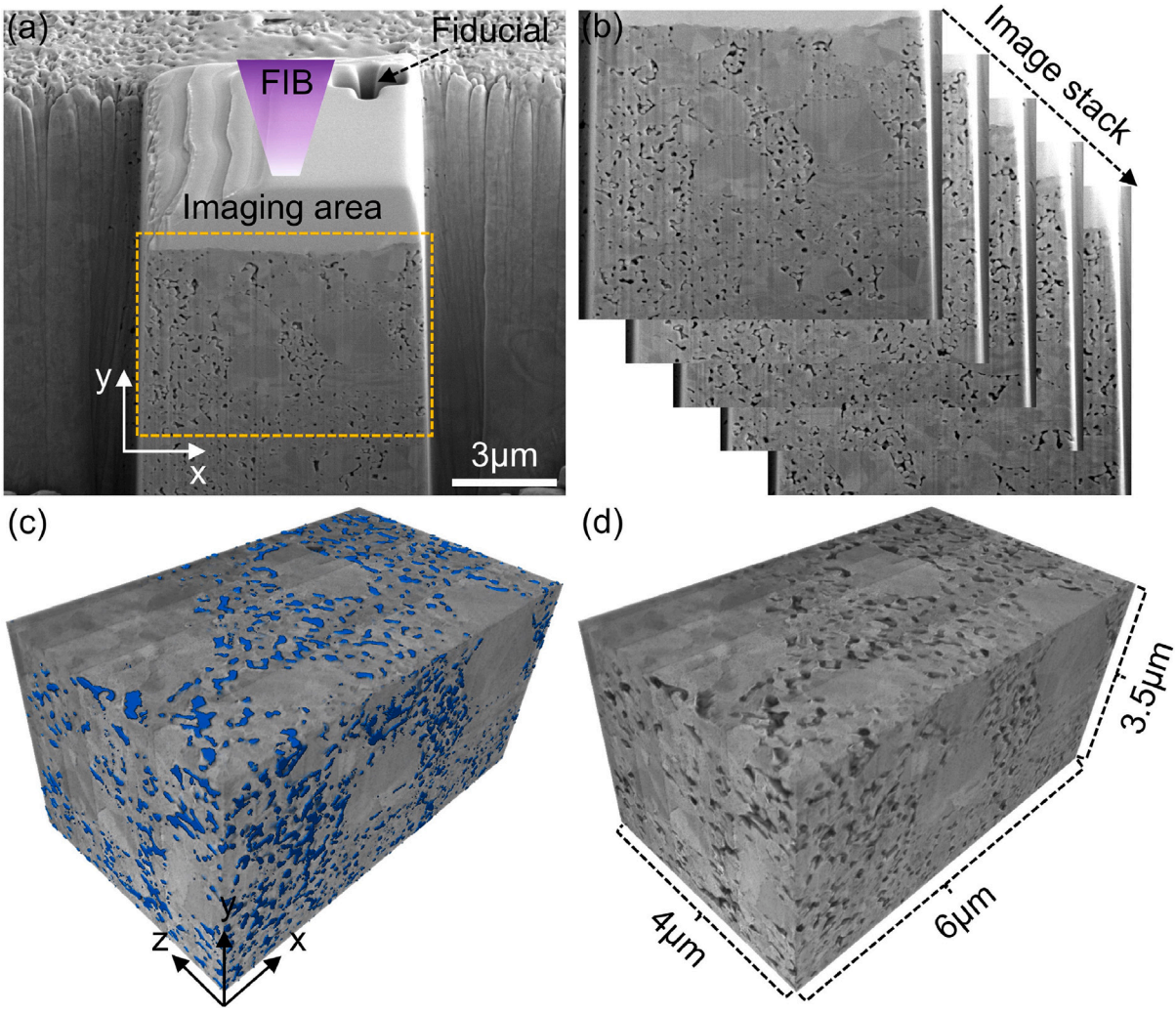

Fig. 3. (a) FIB milling of the sample with a protective Pt layer deposited; the imaging area is indicated; (b) sequential SEM cross-sections forming an image stack for 3D reconstruction; (c) reconstructed volume highlighting porous regions (blue); (d) sintered Cu NP domain with dimensions. (For interpretation of the references to color in this figure legend, the reader is referred to the web version of this article.)

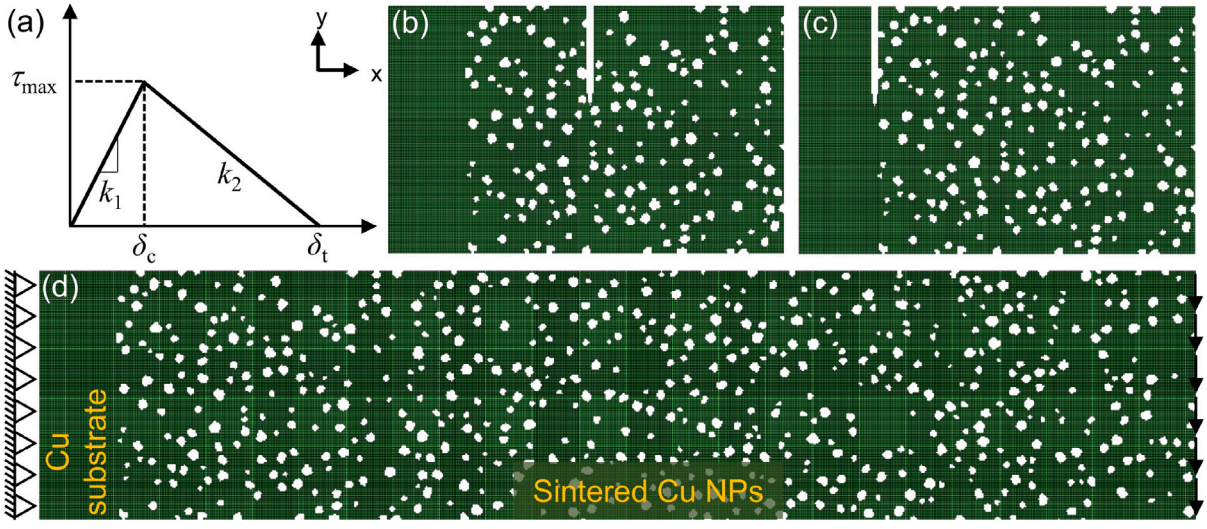

Fig. 4. (a) Typical bilinear law of CZM; (b) Cu NP-notched model; (c) interface-notched model; (d) un-notched model with boundary conditions.

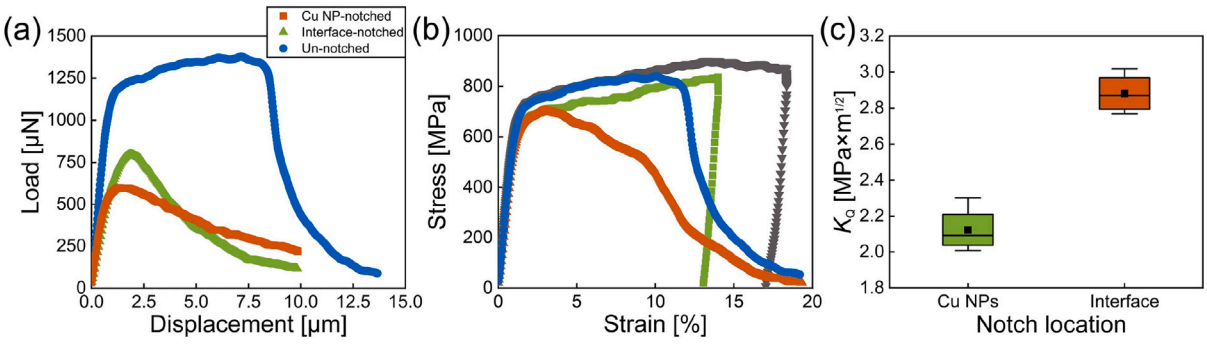

Fig. 5. (a) Load–displacement curves; (b) stress–strain curves of un-notched micro-cantilevers; (c) stress intensity factors.

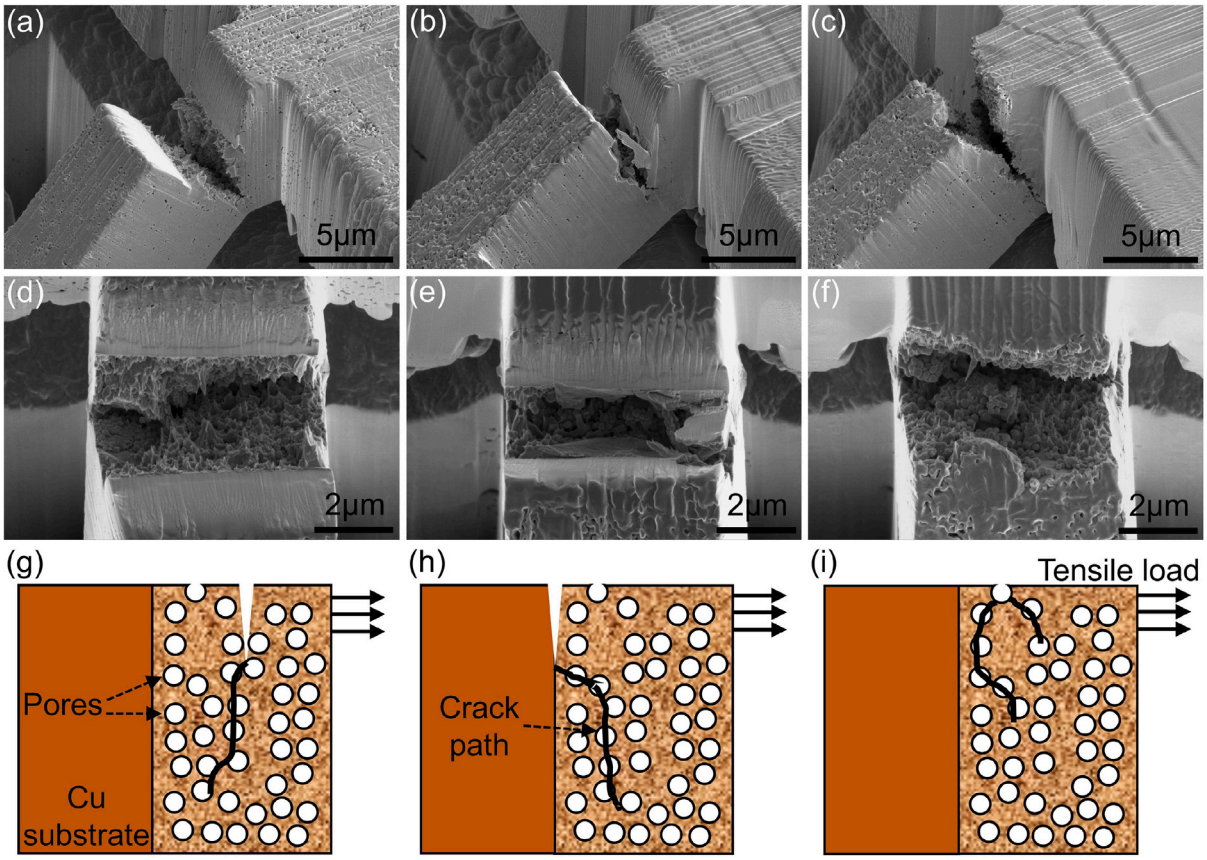

Fig. 6. Fracture morphology and crack propagation in sintered Cu NP micro-cantilevers: (a, d) NP-notched; (b, e) interface-notched; (c, f) un-notched specimens. (g-i) Schematics of corresponding crack propagation mechanisms.

where F, L_b, w and B denote the applied force, moment arm, beam width and thickness, respectively. The corresponding stress–strain curves are shown in Fig. 5b. The measured elastic modulus of approximately 54 ± 2.4 GPa is consistent with values reported for sintered NPs [28] but lower than those observed in Cu thin films and single-crystal Cu micro-cantilevers [72,73]. Similarly, the yield stress, determined via the 0.2% offset criterion [70] to be 639 ± 29 MPa, agrees well with prior micro-cantilever bending studies on sintered Cu NPs [28]. In contrast, this value exceeds reported yield strengths for bulk Cu—derived from micro-cantilever bending [74], compression [75], and shear tests [76], which typically range from 180 to 350 MPa, depending on grain size and crystallographic orientation.

As illustrated in Fig. 5a, interface-notched micro-cantilevers exhibit superior mechanical performance to those NP-notched micro-cantilevers, suggesting enhanced interfacial integrity and crack propagation resistance at the interface. To quantitatively evaluate the fracture resistance, the stress intensity factor K_Q (conditional fracture toughness) was computed based on linear elastic fracture mechanics (LEFM) in mode I [27,77].

$$K_Q = \frac{F L_b}{W \cdot B^{3/2}} \cdot f\left(\frac{a}{B}\right) \tag{6}$$

The geometry factor f was derived as a function of crack length and micro-cantilever height, utilizing finite element (FE) modeling data provided by Iqbal et al. [78]. This analysis standardizes the load–displacement data, enabling direct comparison of fracture behavior across different micro-cantilever configurations. As shown in Fig. 5c,

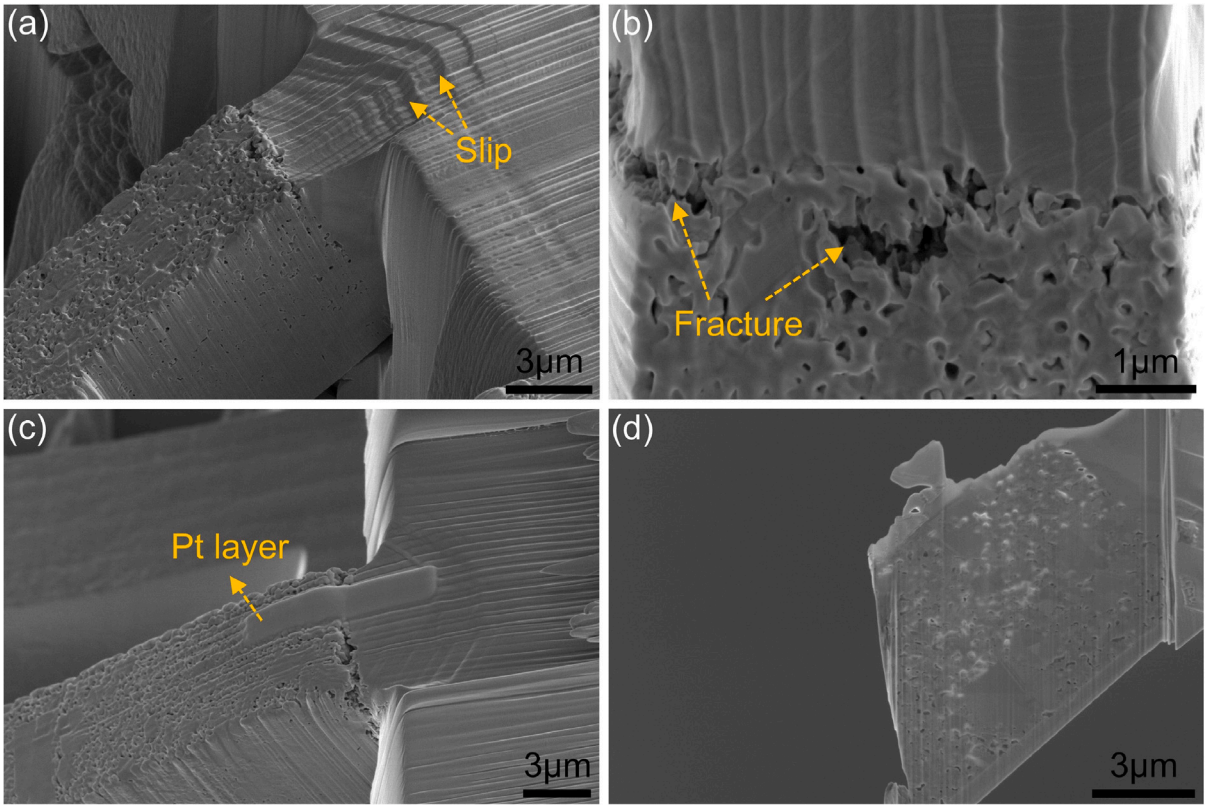

Fig. 7. Deformation behavior of un-notched micro-cantilevers: (a, b) Crack propagation through sintered Cu NPs with concurrent slip deformation in Cu substrate; (c) TEM sample preparation location; (d) fabricated TEM sample.

the stress intensity factor for NP-notched micro-cantilevers is approximately 2.12 ± 0.11 MPa $m^{1/2}$, which is notably lower than the 2.88 ± 0.10 MPa $m^{1/2}$ measured for interface-notched micro-cantilevers.

The disparity in K_Q values highlights the superior crack resistance at the Cu substrate-Cu NP interface, which serves as a more effective barrier to crack propagation compared to the sintered Cu NPs. These findings strongly support the feasibility of all-Cu integration, as the superior interface strength ensures improved mechanical reliability. To investigate the strengthening mechanisms underlying the interfacial fracture toughness of the sintered Cu NPs, crack propagation and localized deformation mechanism were systematically analyzed in next parts.

3.2. Fracture analysis

Fig. 6 delineates the fracture mechanisms of the three micro-cantilever configurations subjected to bending. In notched specimens (Figs. 6a, b, d and e), crack propagation preferentially follows the sintered Cu NPs, evidenced by elongated sintering necks—a hallmark of ductile fracture. Notably, interface-notched micro-cantilevers exhibit a higher critical stress intensity factor (2.88 ± 0.10 MPa $m^{1/2}$) than those NP-notched micro-cantilevers (2.12 ± 0.11 MPa $m^{1/2}$). This disparity stems from microstructural heterogeneity: NP-notched micro-cantilevers (Figs. 6a, d) display elevated porosity distribution near the notch tip than interface-notched micro-cantilevers. Increased porosity amplifies localized stress concentrations, reducing fracture resistance and accelerating crack propagation through the porous NP matrix.

Un-notched micro-cantilevers (Figs. 6c, f) further validate this mechanism. Crack paths deviate from the Cu-substrate interface, instead propagating through the sintered Cu NPs. This deflection underscores the dominance of stress concentrations within the porous NP layer over interfacial adhesion, confirming the sintered NPs' lower cohesive strength compared to the monolithic Cu substrate. Complementary schematics (Figs. 6g–i) illustrate how porosity governs crack initiation and growth, with stress concentrations nucleating at high-porosity regions and propagation modulated by the sintered network's tortuosity. These findings emphasize the critical role of microstructural defects in dictating fracture resistance in hierarchical systems.

Figs. 7a and b reveals a synergistic deformation mechanism in un-notched micro-cantilevers, where crack propagation through the sintered Cu NPs coexists with plastic slip deformation in the Cu substrate. The substrate (Fig. 7a) exhibits distinct slip bands, indicative of dislocation glide under tensile bending stresses. Concurrently, the NP layer (Fig. 7b) undergoes crack propagation preceded by localized plastic deformation, evidenced by elongated sintering necks. This dual behavior highlights mechanical compatibility: the substrate accommodates strain via crystallographic slip, while the NP layer redistributes stress through ductile neck elongation prior to fracture.

The absence of interfacial delamination confirms robust bonding between the NPs and substrate. However, fracture localization within the NP layer demonstrates that residual porosity and microstructural heterogeneities (e.g., incomplete sintering necks) act as preferential stress concentrators, overriding the interfacial adhesion strength. This underscores the sintered Cu NPs' role as the performance-limiting phase, constrained by their inherent porosity. The coexistence of substrate plasticity and NP-layer cracking further suggests that sintering parameters must be optimized to enhance neck connectivity, thereby improving load-transfer efficiency without compromising interfacial integrity.

3.3. Interfacial deformation mechanisms

To elucidate the microstructural and interfacial deformation mechanisms in sintered Cu NP systems, a correlative analysis was conducted using TEM and TKD. Investigations were focused on two representative regions: an undeformed interface, and a deformed interface located at

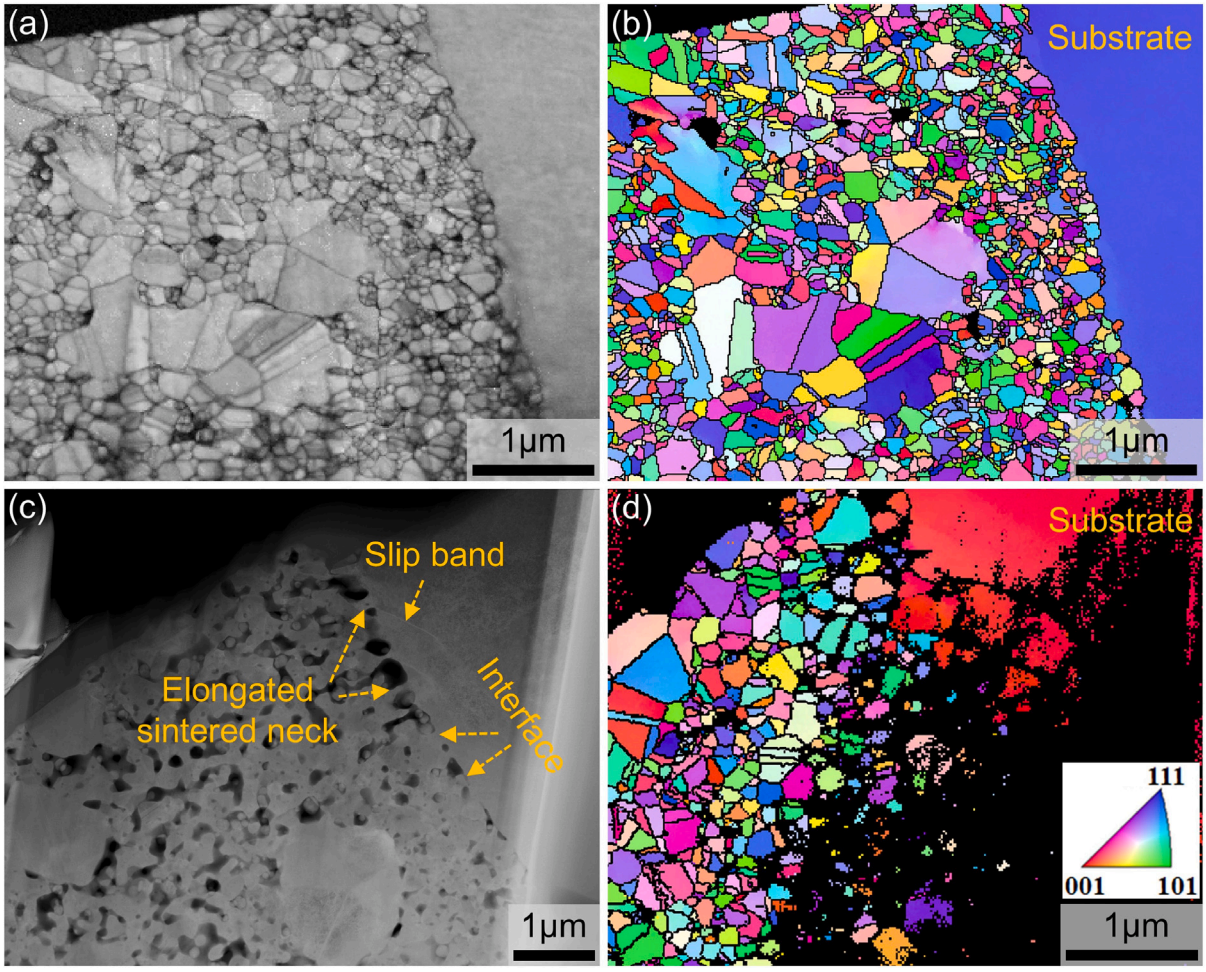

Fig. 8. Grain orientation analysis of sintered Cu NPs at the interface: (a) TKD band contrast map showing pattern quality; (b) initial grain orientation map; (c) bright-field TEM image of deformed region with slip bands and elongated sintered necks; (d) post-deformation grain orientation map.

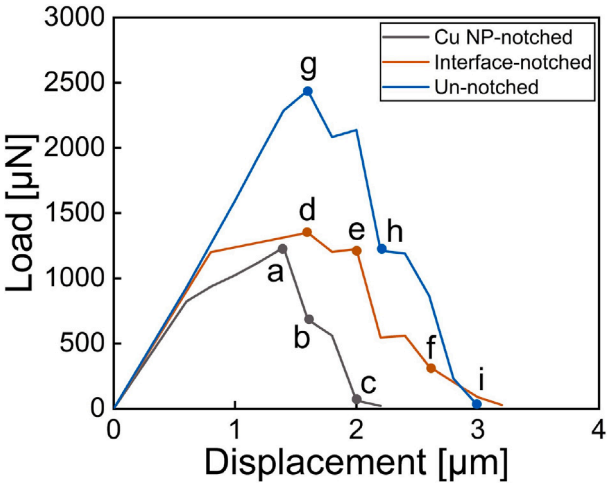

Fig. 9. Load–displacement curves.

the root of a bent micro-cantilever (Figs. 7c, d and S3). TKD mapping of the undeformed region (Figs. 8a, b) revealed a randomized grain orientation distribution within the sintered Cu NPs, indicative of the absence of preferential crystallographic alignment. This structural randomness, coupled with a minimal presence of interfacial voids or discontinuities, suggests the formation of robust metallurgical bonding between the sintered NPs and the underlying Cu substrate.

Post-deformation analyses of the interfacial region (Figs. 8c, d) reveal substantial microstructural reorganization within the NP layer. Bright-field TEM imaging (Fig. 8c) confirms the occurrence of localized plastic deformation, manifested by the elongation of sintering necks. This morphological evolution is attributed to stress concentrations facilitated by the intrinsic porosity of the sintered network. Simultaneously, the appearance of slip bands within the Cu substrate (Fig. 8c) reflects the activation of dislocation glide, a primary plastic deformation mechanism in face-centered cubic (FCC) metals subjected to tensile stress [79,80]. The corresponding TKD map (Fig. 8d) illustrates a heterogeneous grain structure, characterized by a mixture of equiaxed and elongated nanograins, along with deformation-induced lattice distortions that adversely affect diffraction pattern quality. These distortions—likely stemming from dislocation tangles and residual stress accumulation—complicate orientation indexing and highlight the intrinsic difficulty of characterizing highly strained microstructures.

Importantly, deformation twinning was observed in the substrate (Figs. 8c, d), signifying the activation of secondary plastic deformation mechanisms under bending stress. Despite the evident plasticity and microstructural evolution within the sintered NP layer, the integrity of the particle–substrate interface remained preserved. These results emphasize the necessity of optimizing sintering parameters – such as the application of external pressure during processing – to reduce porosity, enhance interparticle neck growth, and ultimately improve the mechanical load-bearing performance of the sintered NP layer without compromising interfacial cohesion.

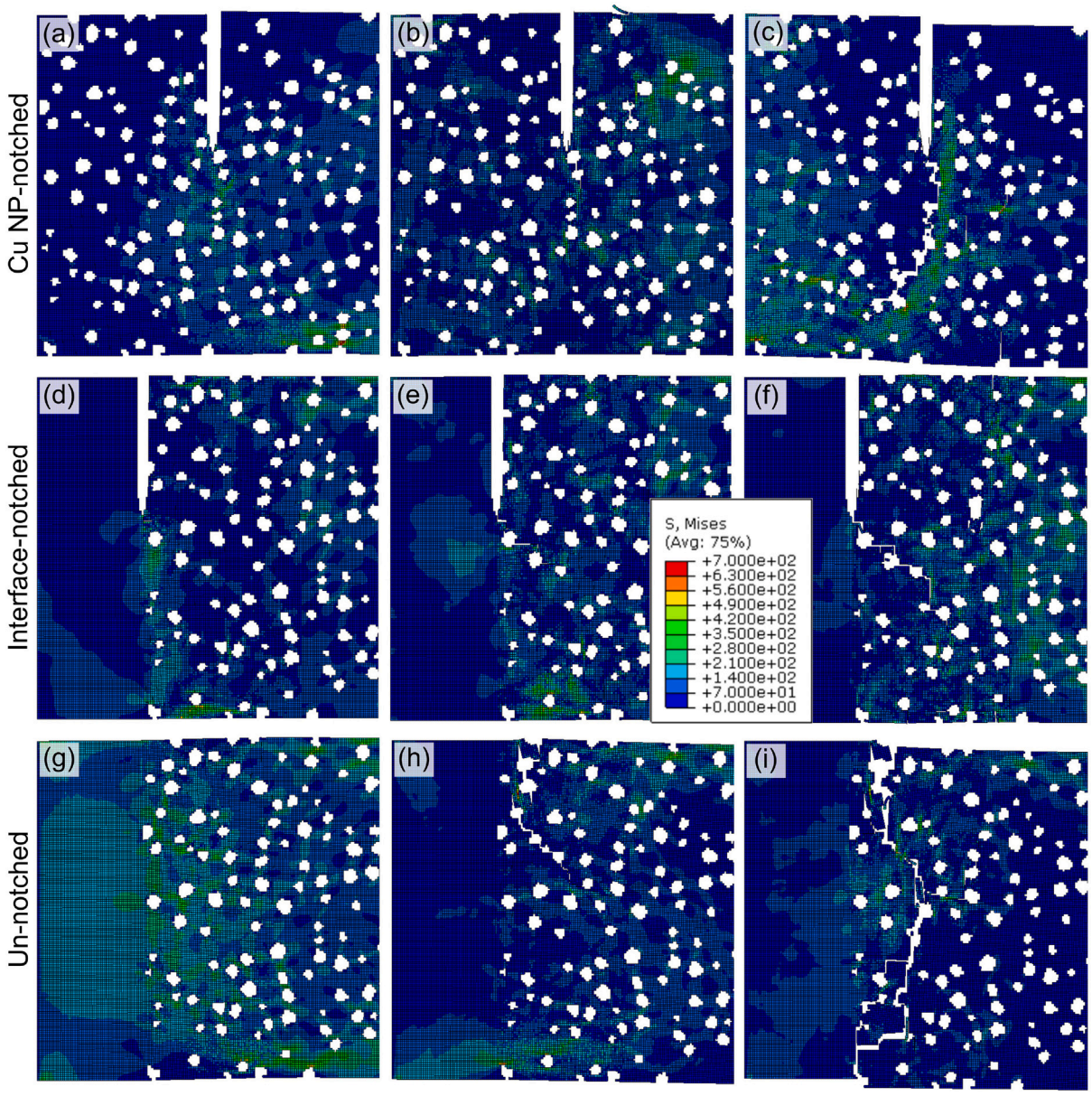

Fig. 10. Crack propagation path and distributions of von Mises stress: (a-c) Cu NP-notched micro-cantilever (a, 0–728 MPa; b, 0–601 MPa; c, 0–696 MPa); (d-f) interface-notched micro-cantilever (d, 0–569 MPa; e, 0–598 MPa; f, 0–650 MPa); (g-i) un-notched micro-cantilever (g, 0–725 MPa; h, 0–678 MPa; i, 0–735 MPa).

3.4. Numerical simulation of crack propagation

Fig. 9 illustrates the load–displacement responses obtained from the simulation, highlighting the influence of notch location. For Cu NP-notched micro-cantilevers, the load–displacement curve demonstrates a significantly lower peak value. In contrast, interface-notched micro-cantilevers exhibits higher strength due to fewer voids, indicating that interface bonding plays a crucial role in mechanical integrity. The un-notched micro-cantilevers achieve the highest load values. These findings align well with experimental results presented in Fig. 5, confirming the influence of void distribution and notch location on strength.

Fig. 10 provides a detailed view of crack propagation path and von Mises stress distribution, revealing localized stress concentrations that act as precursors to crack initiation. The subfigures in Fig. 10 corresponds to the points on the load–displacement curves shown in Fig. 9. The results underscore the significant role of voids in crack propagation, consistent with findings on sintered Ag NPs [27], where porosity governs fracture paths and reduces structural stability. Similar to observations by Su et al. [36] and Chen et al. [27], the porous distribution in sintered Cu NPs creates stress hot spots that accelerate failure. The observed stress localization emphasizes the need to optimize sintering parameters, such as pressure and temperature, to minimize porosity, improve sintering neck formation and enhance mechanical uniformity.

The agreement between CZM and experimental results (Figs. 6 and 7) further validates these observations. Fracture morphologies in Fig. 6 depict crack propagation through porous regions and weakened sintering necks, paralleling the CZM predictions. Additionally, the elongated sintered Cu NPs and localized deformation near stress concentrators observed in Fig. 7 align with the stress patterns in Fig. 10. The presence of porosity in the sintered Cu NPs introduces stress concentrators, reducing overall structural stability. In conclusion, this analysis highlights the robust bonding and effective stress transfer at the Cu substrate interface, reinforcing the feasibility of directly sintering Cu NPs onto a Cu substrate without additional coatings. This approach ensures mechanically reliable, all-Cu integration, making it highly promising for advanced electronic packaging applications.

4. Conclusion

In this study, the interface strength and fracture behavior of sintered Cu NPs were systematically investigated using micro-cantilever bending tests, SEM, TEM, TKD and CZM. This integrated experimental and computational approach enabled a comprehensive analysis of crack initiation and propagation mechanisms of sintered Cu NPs. The main conclusions are as follows:

1. The Cu substrate-sintered Cu NP interface exhibits higher fracture resistance than the sintered Cu NPs, with a stress intensity factor K_Q of approximately 2.88 ± 0.10 MPa $m^{1/2}$ compared to 2.12 ± 0.11 MPa $m^{1/2}$ for cracks propagating within the sintered Cu NPs. This highlights the robust bonding and effective stress transfer at the interface, supporting the feasibility of direct sintering of Cu NPs to a Cu substrate without the need for other coating.

2. Fracture surface analyses reveal that in both types of notched micro-cantilevers, crack propagation preferentially follows the sintered Cu NPs, evidenced by elongated sintering necks. For un-notched micro-cantilevers, interestingly, synergistic deformation mechanism in un-notched micro-cantilevers, where crack propagation through the sintered Cu NPs coexists with plastic slip deformation in the Cu substrate.

3. TKD analysis demonstrates that the sintered Cu NPs exhibit random crystallographic orientations, while the negligible interfacial void density indicates robust metallurgical bonding with the underlying Cu substrate. Complementary TEM and TKD characterization reveals substrate plastic deformation through both slip band formation and sintering neck elongation at the interface.

4. CZM results demonstrate that notch location significantly impacts mechanical properties. Cu NP-notched micro-cantilevers exhibit lower fracture resistance due to increased porosity and stress concentrations, while interface-notched micro-cantilevers show higher strength, attributed to robust bonding and reduced void distribution. Cracks predominantly bypass the interface, propagating through porous regions in the sintered Cu NPs, demonstrating the interface's ability to effectively transfer stress and resist fracture. This performance underscores the potential of direct sintering of Cu NPs onto Cu substrates as a reliable and efficient method for all-Cu integration, without requiring additional coatings, for advanced applications in microelectronics and packaging technologies.

CRediT authorship contribution statement

Leiming Du: Writing – original draft, Validation, Methodology, Investigation, Formal analysis, Data curation, Conceptualization. **Weiping Jiao:** Resources, Investigation. **Olof Bäcke:** Resources, Investigation. **Magnus Hörnqvist Colliander:** Resources, Investigation. **René H. Poelma:** Supervision, Resources, Funding acquisition. **Jiajie Fan:** Writing – review & editing, Supervision, Resources, Investigation. **Willem D. van Driel:** Writing – review & editing, Supervision. **Xuejun Fan:** Supervision, Investigation. **Guoqi Zhang:** Writing – review & editing, Validation, Supervision, Funding acquisition.

Declaration of competing interest

The authors declare that they have no known competing financial interests or personal relationships that could have appeared to influence the work reported in this paper.

Acknowledgments

The authors would like to acknowledge the financial support from the ECSEL Joint Undertaking (JU) under grant agreement No 876659. The JU receives support from the European Union's Horizon 2020 research and innovation program and Germany, Austria, Slovakia, Sweden, Finland, Belgium, Italy, Spain, Netherlands, Slovenia, Greece, France, and Turkey. For the Titan TEM results, we acknowledge support from the Kavli Institute of Nanoscience, Delft University of Technology, and the Netherlands Electron Microscopy Infrastructure (NEMI), project number 184.034.014, part of the National Roadmap and financed by the Dutch Research Council (NWO). The authors gratefully acknowledge Xuyang Yan (Fudan University) for providing technical support with transmission Kikuchi diffraction (TKD) analysis.

Appendix A. Supplementary data

Supplementary material related to this article can be found online at https://doi.org/10.1016/j.actamat.2025.121187.

References

[1] L. Del Carro, J. Zürcher, U. Drechsler, I.E. Clark, G. Ramos, T. Brunschwiler, Low-temperature dip-based all-copper interconnects formed by pressure-assisted sintering of copper nanoparticles, IEEE Trans. Compon. Packag. Manuf. Technol. 9 (8) (2019) 1613–1622.

[2] S. Wang, G. Zou, Y. Wu, Z. Deng, R. Du, L. Liu, Patterned Cu nanoparticle film for all-Cu interconnection without chemical mechanical polishing pretreatment, IEEE Trans. Compon. Packag. Manuf. Technol. 13 (5) (2023) 604–614.

[3] X. Ji, L. Du, H. Van Zeijl, G. Zhang, J. Derakhshandeh, E. Beyne, 20 μm pitch Cu-to-Cu flip-chip interconnects through Cu nanoparticles sintering, in: 2024 IEEE 74th Electronic Components and Technology Conference, ECTC, IEEE, 2024, pp. 1891–1895.

[4] S. Wang, G. Zou, R. Du, L. Liu, Transferring fine-pitch Cu nanoparticle bumps for low-temperature Cu-Cu bonding in chip-scale integration, IEEE Trans. Compon. Packag. Manuf. Technol. (2025).

[5] B.H. Lee, M.Z. Ng, A.A. Zinn, C.L. Gan, Application of copper nanoparticles as die attachment for high power LED, in: 2015 IEEE 17th Electronics Packaging and Technology Conference, EPTC, IEEE, 2015, pp. 1–5.

[6] H.-J. Huang, X. Wu, M.-B. Zhou, X.-P. Zhang, A highly reliable die bonding approach for high power devices by low temperature pressureless sintering using a novel Cu nanoparticle paste, in: 2020 IEEE 70th Electronic Components and Technology Conference, ECTC, IEEE, 2020, pp. 1697–1702.

[7] D. Dai, J. Qian, J. Li, Y. Huang, Z. Wang, J. Yu, X. Wang, X. Chen, A rapid-sintering Cu-Cu joints with ultrahigh shear strength and super reliability for power electronics package, Mater. Sci. Semicond. Process. 178 (2024) 108405.

[8] T.-C. Chou, K.-M. Yang, J.-C. Li, T.-Y. Yu, Y.-T. Yang, H.-W. Hu, Y.-W. Liu, C.-T. Ko, Y.-H. Chen, T.-J. Tseng, et al., Investigation of pillar–concave structure for low-temperature Cu–Cu direct bonding in 3-D/2.5-D heterogeneous integration, IEEE Trans. Compon. Packag. Manuf. Technol. 10 (8) (2020) 1296–1303.

[9] D. Liu, T.-Y. Kuo, Y.-W. Liu, Z.-J. Hong, Y.-T. Chung, T.-C. Chou, H.-W. Hu, K.-N. Chen, Investigation of low-temperature Cu–Cu direct bonding with Pt passivation layer in 3-D integration, IEEE Trans. Compon. Packag. Manuf. Technol. 11 (4) (2021) 573–578.

[10] C. He, J. Zhou, R. Zhou, C. Chen, S. Jing, K. Mu, Y.-T. Huang, C.-C. Chung, S.-J. Cherng, Y. Lu, et al., Nanocrystalline copper for direct copper-to-copper bonding with improved cross-interface formation at low thermal budget, Nat. Commun. 15 (1) (2024) 7095.

[11] C.-J. Du, X. Li, Y.-H. Mei, G.-Q. Lu, An explanation of sintered silver bonding formation on bare copper substrate in air, Appl. Surf. Sci. 490 (2019) 403–410.

[12] D. Yamagiwa, T. Matsuda, H. Furusawa, K. Sato, H. Tatsumi, T. Sano, Y. Kashiba, A. Hirose, Pressureless sinter joining of bare Cu substrates under forming gas atmosphere by surface-oxidized submicron Cu particles, J. Mater. Sci., Mater. Electron. 32 (14) (2021) 19031–19041.

[13] K. Matoy, T. Detzel, M. Müller, C. Motz, G. Dehm, Interface fracture properties of thin films studied by using the micro-cantilever deflection technique, Surf. Coat. Technol. 204 (6–7) (2009) 878–881.

[14] G. Otieno, A. Koos, F. Dillon, N.A. Yahya, C.E. Dancer, G.M. Hughes, N. Grobert, R.I. Todd, Stiffness, strength and interwall sliding in aligned and continuous multi-walled carbon nanotube/glass composite microcantilevers, Acta Mater. 100 (2015) 118–125.

[15] S. Massl, W. Thomma, J. Keckes, R. Pippan, Investigation of fracture properties of magnetron-sputtered TiN films by means of a FIB-based cantilever bending technique, Acta Mater. 57 (6) (2009) 1768–1776.

[16] G. Dehm, B.N. Jaya, R. Raghavan, C. Kirchlechner, Overview on micro-and nanomechanical testing: New insights in interface plasticity and fracture at small length scales, Acta Mater. 142 (2018) 248–282.

[17] R. Daniel, M. Meindlhumer, W. Baumegger, J. Zalesak, B. Sartory, M. Burghammer, C. Mitterer, J. Keckes, Grain boundary design of thin films: using tilted brittle interfaces for multiple crack deflection toughening, Acta Mater. 122 (2017) 130–137.

[18] J. Tatami, Y. Imoto, T. Yahagi, T. Takahashi, M. Iijima, Relationship between bending strength of bulk porous silicon carbide ceramics and grain boundary strength measured using microcantilever beam specimens, J. Eur. Ceram. Soc. 40 (7) (2020) 2634–2641.

[19] R. Henry, H. Saad, A. Doitrand, S. Deville, S. Meille, Interface failure in nacre-like alumina, J. Eur. Ceram. Soc. 40 (13) (2020) 4694–4699.
[20] J. Ast, M. Ghidelli, K. Durst, M. Göken, M. Sebastiani, A.M. Korsunsky, A review of experimental approaches to fracture toughness evaluation at the micro-scale, Mater. Des. 173 (2019) 107762.
[21] S. Heuer, B.-S. Li, D. Armstrong, Y. Zayachuk, C. Linsmeier, Microstructural and micromechanical assessment of aged ultra-fast sintered functionally graded iron/tungsten composites, Mater. Des. 191 (2020) 108652.
[22] A.H. Iyer, P. Gupta, P. Gudmundson, A. Kulachenko, Measuring microscale mechanical properties of PVdF binder phase and the binder-particle interface using micromechanical testing, Mater. Sci. Eng.: A 881 (2023) 145352.
[23] D. Armstrong, A. Wilkinson, S. Roberts, Micro-mechanical measurements of fracture toughness of bismuth embrittled copper grain boundaries, Phil. Mag. Lett. 91 (6) (2011) 394–400.
[24] D. Hu, C. Qian, X. Liu, L. Du, Z. Sun, X. Fan, G. Zhang, J. Fan, High temperature viscoplastic deformation behavior of sintered nanocopper paste used in power electronics packaging: insights from constitutive and multi-scale modelling, J. Mater. Res. Technol. 26 (2023) 3183–3200.
[25] K. Wakamoto, D. Yasugi, T. Otsuka, K. Nakahara, T. Namazu, Fracture mechanism of sintered silver film revealed by in-situ SEM uniaxial tensile loading, IEEE Trans. Compon.Packag. Manuf. Technol. (2024).
[26] C. Chen, K. Suganuma, Microstructure and mechanical properties of sintered ag particles with flake and spherical shape from nano to micro size, Mater. Des. 162 (2019) 311–321.
[27] C. Chen, S. Nagao, K. Suganuma, J. Jiu, T. Sugahara, H. Zhang, T. Iwashige, K. Sugiura, K. Tsuruta, Macroscale and microscale fracture toughness of microporous sintered Ag for applications in power electronic devices, Acta Mater. 129 (2017) 41–51.
[28] D. Hu, L. Du, M. Alfreider, J. Fan, D. Kiener, G. Zhang, Microscopic fracture toughness of notched porous sintered Cu micro-cantilevers for power electronics packaging, Mater. Sci. Eng.: A 897 (2024) 146316.
[29] J. Liu, H. Chen, H. Ji, M. Li, Highly conductive Cu–Cu joint formation by low-temperature sintering of formic acid-treated Cu nanoparticles, ACS Appl. Mater. Interfaces 8 (48) (2016) 33289–33298.
[30] E. Martínez-Pañeda, A. Golahmar, C.F. Niordson, A phase field formulation for hydrogen assisted cracking, Comput. Methods Appl. Mech. Engrg. 342 (2018) 742–761.
[31] M. Dittmann, F. Aldakheel, J. Schulte, F. Schmidt, M. Krüger, P. Wriggers, C. Hesch, Phase-field modeling of porous-ductile fracture in non-linear thermo-elasto-plastic solids, Comput. Methods Appl. Mech. Engrg. 361 (2020) 112730.
[32] B. He, L. Schuler, P. Newell, A numerical-homogenization based phase-field fracture modeling of linear elastic heterogeneous porous media, Comput. Mater. Sci. 176 (2020) 109519.
[33] B. He, T. Vo, P. Newell, Investigation of fracture in porous materials: a phase-field fracture study informed by ReaxFF, Eng. Comput. 38 (2022) 5617–5633.
[34] H. Hu, L. Qi, X. Chao, Physics-informed neural networks (PINN) for computational solid mechanics: Numerical frameworks and applications, Thin-Walled Struct. (2024) 112495.
[35] Y. Su, G. Fu, C. Liu, K. Zhang, L. Zhao, C. Liu, A. Liu, J. Song, Thermo-elasto-plastic phase-field modelling of mechanical behaviours of sintered nano-silver with randomly distributed micro-pores, Comput. Methods Appl. Mech. Engrg. 378 (2021) 113729.
[36] Y. Su, J. Zhu, X. Long, L. Zhao, C. Chen, C. Liu, Statistical effects of pore features on mechanical properties and fracture behaviors of heterogeneous random porous materials by phase-field modeling, Int. J. Solids Struct. 264 (2023) 112098.
[37] Y. Su, Z. Shen, X. Long, C. Chen, L. Qi, X. Chao, Gaussian filtering method of evaluating the elastic/elasto-plastic properties of sintered nanocomposites with quasi-continuous volume distribution, Mater. Sci. Eng.: A 872 (2023) 145001.
[38] N. Moës, J. Dolbow, T. Belytschko, A finite element method for crack growth without remeshing, Internat. J. Numer. Methods Engrg. 46 (1) (1999) 131–150.
[39] F. Xu, H. Hajibeygi, L.J. Sluys, Multiscale extended finite element method for deformable fractured porous media, J. Comput. Phys. 436 (2021) 110287.
[40] A.R. Khoei, M. Vahab, E. Haghighat, S. Moallemi, A mesh-independent finite element formulation for modeling crack growth in saturated porous media based on an enriched-FEM technique, Int. J. Fract. 188 (2014) 79–108.
[41] R. Verma, P. Kumar, R. Jayaganthan, H. Pathak, Extended finite element simulation on tensile, fracture toughness and fatigue crack growth behaviour of additively manufactured Ti6Al4V alloy, Theor. Appl. Fract. Mech. 117 (2022) 103163.
[42] A. Muixí, O. Marco, A. Rodríguez-Ferran, S. Fernández-Méndez, A combined XFEM phase-field computational model for crack growth without remeshing, Comput. Mech. 67 (2021) 231–249.
[43] M. Nikolić, Discrete element model for the failure analysis of partially saturated porous media with propagating cracks represented with embedded strong discontinuities, Comput. Methods Appl. Mech. Engrg. 390 (2022) 114482.
[44] Z. Wang, L. Yang, S. Zhu, W.-L. Song, H.-S. Chen, Exploring mechanical failure of porous electrode meso structure using the discrete element method, Extrem. Mech. Lett. 46 (2021) 101252.
[45] R.H. Moghaddam, A. Golshani, Fatigue behavior investigation of artificial rock under cyclic loading by using discrete element method, Eng. Fail. Anal. 160 (2024) 108105.
[46] J. Zhang, Y. Chen, R. Du, X. Zhao, J. Wu, Macroscopic and microscopic mechanical characteristics and crack propagation behavior of sandstone-like samples with single cracks under freeze–thaw cycles: experimental and numerical simulation, Theor. Appl. Fract. Mech. 129 (2024) 104201.
[47] S. Zhao, Y. Dai, F. Qin, Y. Li, L. Liu, Z. Zan, T. An, P. Chen, Y. Gong, Y. Wang, On mode II fracture toughness of sintered silver based on end-notch flexure (ENF) test considering various sintering parameters, Mater. Sci. Eng.: A 823 (2021) 141729.
[48] J. Wei, Y. Dai, F. Qin, Inverse identification of cohesive zone parameters for sintered nano-silver joints based on dynamic convolution neural network, Eng. Fract. Mech. 292 (2023) 109651.
[49] Y. Dai, Y. Li, Z. Zan, F. Qin, Bondline thickness effect on fracture and cohesive zone model of sintered nano silver adhesive joints under end notched flexure tests, Fatigue Fract. Eng. Mater. Struct. 46 (6) (2023) 2062–2079.
[50] Y. Dai, Z. Zan, S. Zhao, F. Qin, Mode II cohesive zone law of porous sintered silver joints with nickel coated multiwall carbon nanotube additive under ENF test, Theor. Appl. Fract. Mech. 121 (2022) 103498.
[51] Y. Wang, J. Li, Phase field modeling of defects and deformation, Acta Mater. 58 (4) (2010) 1212–1235.
[52] T.-T. Nguyen, J. Yvonnet, D. Waldmann, Q.-C. He, Phase field modeling of interfacial damage in heterogeneous media with stiff and soft interphases, Eng. Fract. Mech. 218 (2019) 106574.
[53] J. Zambrano, S. Toro, P. Sánchez, F. Duda, C. Méndez, A. Huespe, Interaction analysis between a propagating crack and an interface: Phase field and cohesive surface models, Int. J. Plast. 156 (2022) 103341.
[54] C.A. Duarte, D.-J. Kim, Analysis and applications of a generalized finite element method with global–local enrichment functions, Comput. Methods Appl. Mech. Engrg. 197 (6–8) (2008) 487–504.
[55] D. Xu, Z. Liu, X. Liu, Q. Zeng, Z. Zhuang, Modeling of dynamic crack branching by enhanced extended finite element method, Comput. Mech. 54 (2014) 489–502.
[56] J.E. Andrade, U. Mital, Multiscale and multiphysics modeling of soils, in: Geotechnical fundamentals for addressing new world challenges, Springer, 2019, pp. 141–168.
[57] W. Chen, X. Liu, D. Hu, X. Zhu, X. Fan, G. Zhang, J. Fan, Unraveling the hydrogen sulfide aging mechanism on electrical-thermal–mechanical property degradation of sintered nanocopper interconnects used in power electronics packaging, Mater. Des. 238 (2024) 112702.
[58] J. Ast, M.N. Polyakov, G. Mohanty, J. Michler, X. Maeder, Interplay of stresses, plasticity at crack tips and small sample dimensions revealed by in-situ microcantilever tests in tungsten, Mater. Sci. Eng.: A 710 (2018) 400–412.
[59] A.H. Iyer, K. Stiller, M.H. Colliander, Room temperature plasticity in thermally grown sub-micron oxide scales revealed by micro-cantilever bending, Scr. Mater. 144 (2018) 9–12.
[60] L. Du, K. Liu, D. Hu, O. Bäcke, X. Hu, X. Ji, J. Fan, R.H. Poelma, M.H. Colliander, G. Zhang, Microstructural and mechanical anisotropy in pressure-assisted sintered copper nanoparticles, Acta Mater. (2025) 120772.
[61] R. Zhu, G. Niu, Z. Qu, P. Wang, R. Zhang, D. Fang, In-situ quantitative tracking of micro-crack evolution behavior inside CMCs under load at high temperature: a deep learning method, Acta Mater. 255 (2023) 119073.
[62] S.N. Kumaran, S.K. Sahoo, C. Haase, L.A. Barrales-Mora, L.S. Toth, Nanostructuring of a high entropy alloy by severe plastic deformation: Experiments and crystal plasticity simulations, Acta Mater. 250 (2023) 118814.
[63] S. Park, J.G. Kim, J.B. Seol, H. Sung, et al., Ultrastrong and stress corrosion cracking-resistant martensitic steels, Acta Mater. 239 (2022) 118291.
[64] X. Chao, W. Tian, F. Xu, D. Shou, A fractal model of effective mechanical properties of porous composites, Compos. Sci. Technol. 213 (2021) 108957.
[65] M. Neumann, M. Osenberg, A. Hilger, D. Franzen, T. Turek, I. Manke, V. Schmidt, On a pluri-Gaussian model for three-phase microstructures, with applications to 3D image data of gas-diffusion electrodes, Comput. Mater. Sci. 156 (2019) 325–331.
[66] Y. Gao, Y. Jiao, Y. Liu, Ultra-efficient reconstruction of 3D microstructure and distribution of properties of random heterogeneous materials containing multiple phases, Acta Mater. 204 (2021) 116526.
[67] X. Long, J. Zhu, Y. Su, Y. Yan, C. Chang, H. Zhang, V. Salomoni, Phase field fracture modeling of mechanical degradation and crack propagation in random porous sintered nano-silver with thermal and strain-rate effects, Eng. Fract. Mech. (2024) 110753.
[68] S.T. Mousavi, N. Richart, C. Wolff, J.-F. Molinari, Dynamic crack propagation in a heterogeneous ceramic microstructure, insights from a cohesive model, Acta Mater. 88 (2015) 136–146.
[69] C. Motz, T. Schöberl, R. Pippan, Mechanical properties of micro-sized copper bending beams machined by the focused ion beam technique, Acta Mater. 53 (15) (2005) 4269–4279.
[70] E. Demir, D. Raabe, F. Roters, The mechanical size effect as a mean-field breakdown phenomenon: Example of microscale single crystal beam bending, Acta Mater. 58 (5) (2010) 1876–1886.

[71] M. Wurmshuber, S. Jakob, S. Doppermann, S. Wurster, R. Bodlos, L. Romaner, V. Maier-Kiener, D. Kiener, Tuning mechanical properties of ultrafine-grained tungsten by manipulating grain boundary chemistry, Acta Mater. 232 (2022) 117939.
[72] S.-H. Hong, K. Kim, Y.-M. Kim, J.-H. Hahn, C.-S. Lee, J.-H. Park, Characterization of elastic moduli of Cu thin films using nanoindentation technique, Compos. Sci. Technol. 65 (9) (2005) 1401–1408.
[73] D.E. Armstrong, A.J. Wilkinson, S.G. Roberts, Measuring anisotropy in Young's modulus of copper using microcantilever testing, J. Mater. Res. 24 (2009) 3268–3276.
[74] C. Howard, R. Fritz, M. Alfreider, D. Kiener, P. Hosemann, The influence of microstructure on the cyclic deformation and damage of copper and an oxide dispersion strengthened steel studied via in-situ micro-beam bending, Mater. Sci. Eng.: A 687 (2017) 313–322.
[75] M. Mutoh, T. Nagoshi, T.-F.M. Chang, T. Sato, M. Sone, Micro-compression test using non-tapered micro-pillar of electrodeposited Cu, Microelectron. Eng. 111 (2013) 118–121.
[76] J.G. Gigax, J.K. Baldwin, C.J. Sheehan, S.A. Maloy, N. Li, Microscale shear specimens for evaluating the shear deformation in single-crystal and nanocrystalline Cu and at Cu–Si interfaces, J. Mater. Res. 34 (9) (2019) 1574–1583.
[77] R.O. Ritchie, D. Liu, Introduction to Fracture Mechanics, Elsevier, 2021.
[78] F. Iqbal, J. Ast, M. Göken, K. Durst, In situ micro-cantilever tests to study fracture properties of NiAl single crystals, Acta Mater. 60 (3) (2012) 1193–1200.
[79] A.S. Khan, J. Liu, A deformation mechanism based crystal plasticity model of ultrafine-grained/nanocrystalline FCC polycrystals, Int. J. Plast. 86 (2016) 56–69.
[80] F. Wang, J. Guo, D. Weygand, F. Wang, T.J. Rupert, D. Chen, D.S. Gianola, Topology and evolution of dislocation structures mediated by glissile reactions in face-centered cubic metals, Acta Mater. 268 (2024) 119748.